Micropore characteristics of organic matter pools in cemented and non-cemented podzolic horizons

UNIVERSITÀ DEGLI STUDI DI TORINO

Catoni M., D'Amico E.M., Mittelmeijer-Hazeleger M.C., Rothenberg G., Bonifacio E. (2014). Micropore characteristics of organic matter pools in cemented and non-cemented podzolic horizons. European Journal of Soil Science 65, 763–773. DOI:10.1111/ejss.12173

Micro-pore characteristics of organic matter pools in cemented and non-cemented podzolic horizons.

M. CATONI[a], M. E. D'AMICO[a], M. C. MITTELMEIJER-HAZELEGER[b], G. ROTHENBERG[b] & E. BONIFACIO[a]

[a]*Department of Agricultural, Forest and Food Sciences (DISAFA), University of Torino, Via L. da Vinci 44, 10095, Grugliasco, Italy, and*

[b]*Van 't Hoff Institute for Molecular Sciences (HIMS), University of Amsterdam, Science Park 904, 1098XH, Amsterdam, the Netherlands*

Correspondence: M. Catoni. Email: marcella.catoni@unito.it

Running title: Micro-pore characteristics of OM in podzolic horizons

Summary

In Podzols, organic matter (OM) is stabilized mainly by interaction with minerals, as a direct consequence of pedogenic processes. Metal-organic associations strongly affect OM surface features, particularly micro-porosity. Cemented ortstein horizons (CM) may form during podzolization, accompanied by a spatial arrangement of OM on mineral surfaces which differs from that in non-cemented horizons (N-CM). To investigate the metal-organic associations and their changes during pedogenesis, we selected both N-CM and CM podzolic horizons, isolated NaClO-resistant OM and compared the specific surface area (SSA) before and after OM oxidation. The SSA was assessed by using N_2, to detect the pores in the range of micro-pores (<2 nm) and meso-pores (2–50 nm), and CO_2, to measure a smaller micro-porosity (<0.5 nm), which is not accessible to N_2. Only the N-CM samples showed the typical increase in N_2-SSA after the removal of labile OM, while a decrease was found in all CM horizons. The CO_2-SSA revealed a large number of small micro-pores characterizing OM, both before and after oxidation. The smallest micropore classes (<0.5 nm) were, however, more abundant in NaClO-resistant OM, that had therefore a larger number of N_2-inaccessible surfaces than the labile pool. The N_2-SSA data thus indicated a more homogeneous coverage of mineral surfaces by stabilized OM in CM samples. Because of the abundance of small micro-pores, OM in these podzolic B horizons had extremely large CO_2-SSA values (about 800 $m^2\ g^{-1}$), with sharp differences between the NaClO-labile OM (290–380 $m^2\ g^{-1}$) and the NaClO-stabilized pool (1380–1860 $m^2\ g^{-1}$), thus indicating very reactive illuvial organic materials.

Keywords: CO_2 and N_2 adsorption, specific surface area, soil organic matter stabilization, metal-organic associations, Spodosols.

Introduction

Carbon (C) stored in soil organic matter (OM) represents the world's third largest pool after oceanic and geological pools, with a global reservoir of approximately 1550 Pg C (Lal, 2008). Although soil management has been proposed as a strategy for reducing the rate of atmospheric CO_2 increase, the forms in which organic carbon (OC) occurs in soils need to be understood better before attempting to enhance long-term soil OC storage (Mikutta *et al.*, 2006). The soil capacity to accumulate and preserve OC against microbial and enzymatic degradation is strongly dependent on the presence of stabilized OM pools. Several factors may potentially play an important role in the stabilization process, but one may prevail depending on soil type, vegetation, management practices and environmental conditions (von Lützow *et al.,* 2008). Recent studies showed that the persistence of soil OM is not strictly related to its molecular properties, and indicated the occurrence of other mechanisms that protect it against decomposition (Schmidt *et al.*, 2011). These mechanisms induce a physicochemical protection of the organic molecules, and seem to be directly connected to soil properties and thus to the main processes that occur during pedogenesis. The physicochemical protection is based on the inhibition of OM biochemical degradation *via* organo-mineral interactions, such as sorption on mineral surfaces, complex formation with metals, occlusion within aggregates, and deposition in pores inaccessible to decomposers and extracellular enzymes (Jastrow *et al.*, 2007). Sorption onto mineral surfaces is considered to be the most effective mechanism that protects soil OM against biochemical degradation. Mineral-organic associations can be viewed conceptually as composed of a zonal sequence consisting of (i) a contact zone, where strong bonds between polar organic groups and mineral surfaces occur, (ii) a hydrophobic zone where exchange with the soil solution is easier and (iii) a kinetic zone where cation bridges and other weaker interactions contribute to the retention of organic compounds (Kleber *et al.*, 2007). In this multilayer arrangement, the OM closest to the mineral surface has a more compacted structure than the more distant OM (Wang & Xing, 2005). This gives rise to a large spatial variability of mineral-organic associations at the <50 nm scale, which is poorly represented by the bulk soil OM pool but has a great effect on the mechanisms governing OM stabilization and C cycling (Lehmann *et al.*, 2008).

In sub-soil B horizons, the mineral-associated OM pool is mainly represented (over 90%) by OM interactions with ferrihydrite, Al (hydr)oxides, and crystalline Fe (hydr)oxides (Mikutta *et al.*, 2006). From this point of view, Podzols are particularly interesting as OM complexation with metals is the characteristic process of soil formation. In agreement with most theories, the downward co-migration of metal-organic complexes occurs during podzolization, resulting in a

clear differentiation in the soil profile, with a light-coloured eluvial horizon which overlies a darker illuvial B horizon (Bs or Bhs; IUSS Working Group WRB, 2006) enriched in OM, iron (Fe) and aluminium (Al). The migration of OM into illuvial horizons thus favours the presence of large OC pools at depth, where OM has longer residence times because of the interaction with mineral phases (Jastrow *et al.*, 2007). Indeed, the amount of stabilized OM has been related to the amounts of metal-organic complexes and poorly crystalline Al and Fe (oxy)hydroxides in Podzols (Kleber *et al*., 2005).

During podzolization, cemented ortstein and placic horizons can also form (Bsm or Bhsm; IUSS Working Group WRB, 2006). The genesis of indurated podzolic layers is not precisely understood: the cementation of placic horizons is thought to be mainly related to changes in drainage conditions and redox dynamics of Fe, while the genesis of the ortstein seems more directly linked to the translocation and immobilization of organic Al complexes (Bockheim, 2011). Cementation in ortstein is favoured by minimal root activity and the presence of large contents of coarse fragments which, by decreasing the soil volume, promote the continuity of illuviated cementing agents (Lapen & Wang, 1999). As a consequence, the association between illuviated OM and metal phases should be more intimate than in non-cemented spodic horizons. In addition, the metal-organic interactions are relatively more abundant in the ortstein than in the non-cemented matrix of the same Bs horizons, thus suggesting a selection of stabilized OM forms.

Recently, we found that the characteristics of metal-organic associations change with increasing intensity of podzolization and that the variations can evaluated from the specific surface area determined by N_2 adsorption (Bonifacio *et al*., 2013). The OM removal from the soil is expected to induce an increase in surface area because of the elimination of the small-surface area component, of the enhanced accessibility of N_2 into pores previously filled by OM, and of the exposure of new mineral surfaces caused by the removal of organic cements from aggregates (Kaiser & Guggenberger, 2003; Echeverrìa *et al.*, 1999). However, in our previous experiment we observed that the N_2-detectable surface decreased after a weak NaClO oxidation of the most labile OM pools and that this behaviour was typical only of the most developed spodic horizons (Bonifacio *et al.*, 2013). The NaClO treatment at pH 8 efficiently removes the most labile OM with minimal modifications of the mineral phase (Zimmermann *et al*., 2007), isolating an older OM fraction which is considered stabilized by interactions with the mineral phases (Mikutta *et al.*, 2006). Our previous results indicated that this OM fraction, protected from oxidation, had less N_2-accessible pores than the labile pool, pointing to a variation in the

micro-structural properties of OM that occurs during the stabilization process through interaction with mineral surfaces.

Although, N_2 adsorption has been recommended as a standard method to measure the OM surface area, soil OM typically provides values, as small as <1 $m^2 g^{-1}$ (Sasaki *et al.*, 2007), which are not consistent with the data reported by other methods and with its known strong reactivity (Chiou *et al.*, 1990). This discrepancy is the direct consequence of the micro-porosity extent of OM, which may easily reach dimensions <2 nm, and the extremely slow diffusion of the N_2 molecules into very small-sized pores (<0.5 nm) at the temperature conditions used for the analysis (de Jonge & Mittelmeijer-Hazeleger, 1996). Organic matter resistant to NaClO could therefore have a greater amount of small micro-porosity, in agreement with the denser and less open configuration of OM found after sorption on goethite by Kaiser & Guggenberger (2007).

To investigate OM structure, with emphasis on small micro-porosity, the CO_2 adsorption technique is particularly suitable (de Jonge *et al.*, 2000; de Jonge & Mittelmeijer-Hazeleger, 1996). Although its molecular diameter is similar to that of N_2, CO_2 is capable of penetrating pores <0.5 nm because of the larger operative temperature (273 K compared with 77 K), and CO_2-derived surface areas of materials rich in organic compounds were orders of magnitude larger than the N_2- surface areas.

The aim of this work was to evaluate the surface features of metal-organic associations in Podzols with cemented horizons. More specifically, we wanted to assess the differences, if any, in the small micro-porosity of NaClO-resistant and labile OM and to relate them to the interaction between OM and mineral components, by using cemented horizons as the maximum degree of metal-organic interaction development.

Materials and methods

The samples used in this study were collected from three soils in the Alps of North-western Italy, one in Piemonte (P1) and the other two (P2 and P3) in Valle d'Aosta regions. All soils were clearly identified as Podzols and discernible and well-developed cemented ortstein horizons always occurred (Table 1). From preliminary soil surveys, we found that Podzols with cemented deep horizons were widespread in the area, particularly below sub-alpine coniferous forest and ericaceous heath on sialic glacial till, where slope angles were small enough to preserve soils from intense erosive processes.

The three soil profiles were formed on Pleistocene or early Holocene glacial deposits, mainly composed of gneiss and other quartz-rich metamorphic rocks; the parent material of P2 also included significant amounts of calcschists and black shales. Soils P1 and P3 were developed

under sub-alpine forests with *Vaccinium* spp. and *Rhododendron ferrugineum* L. understory; P1 was dominated by beech (*Fagus sylvatica* L.) and white fir *(Abies alba* Mill.) while P3 was dominated by larch (*Larix decidua* Mill.). The present-day vegetation overlying P2 was a grazed grassland, while the climax vegetation at this phytoclimatic level should be a sub-alpine ericaceous heath.

The non-cemented spodic horizons (N-CM: Bs and/or Bhs) and the underlying cemented ones (CM: Bsm or CBm) were sampled from profile pit walls; materials (2-3 kg) were collected from the whole thickness of the genetic horizons. All CM horizons had a similar degree of cementation and similar structure (abundant vesicular pores and visible cemented coatings on pore and rock surfaces), but varied in colour (Table 1). Thus they presumably differed in the amounts of illuviated metals, silica and OM. None of the horizons contained swelling layer silicates and mineralogy of the clay fraction was dominated by chlorite, illite and randomly interstratified minerals (data not shown).

The soil samples were air-dried and sieved to 2 mm before chemical analyses. Total OC was determined by dry combustion (CE Instruments NA2100 elemental analyser, Rodano, Italy). Acid ammonium oxalate extractable-Fe (Schwertmann, 1964), Al, Mn and Si (Fe_O, Al_O, Mn_O, Si_O) were determined by atomic absorption spectroscopy (Perkin-Elmer 3030, Waltham, Massachusetts), and Fe_O and Al_O were used to calculate the spodic index (SI: $0.5Fe_O+Al_O$; IUSS Working Group WRB, 2006) to assess quantitatively the illuviation processes and for classification purposes. All chemical analyses were triplicated.

To eliminate the most labile OM, four sub-samples from each B horizon were oxidized with NaClO (pH 8) as described by Mikutta *et al.* (2006). This method involves treating the soil samples three times with 6% NaClO and leads to the removal of significant amounts of OM (Kaiser *et al.*, 2002). After oxidation, the samples were washed with deionized water until the conductivity was less than 40 μS cm^{-1} and oven dried at 40° C. Changes in ionic strength influence the conformation of soil OM, but these changes are reversible and organic macro-molecules are fully uncoiled at NaCl concentrations below $1x10^{-3}$ M (i.e. about 80 μS cm^{-1}) (Ghosh & Schnitzer, 1980). The electrical conductivity of the UT samples varied between 21 and 45 μS cm^{-1} (P3-Bsm1 and P3-Bhs, respectively); thus any differential ionic strength effect on OM conformation is unlikely. After the determination of NaClO-resistant OC and extractable-elements, the sub-samples were bulked for physical analyses.

The sample solid phase density (ρ_s) was determined with a MultiVolume Pycnometer 1305 (Micromeritics, Norcross, GA, USA), with 5 replications. The determination of surface properties was carried out on untreated (UT) and NaClO-treated samples (T). Before

measurement of surface properties, both the T and UT samples were finely ground (<0.5 mm) and outgassed at 323 K for at least 16 hours under vacuum (<10^{-4} kPa). Nitrogen adsorption and desorption isotherms were recorded at 77 K with a static volumetric instrument (Thermo Scientific Surfer, Rodano, Italy) which has a combined linearity error of less than 0.1% in the working pressure range. The Brunauer–Emmett–Teller (BET) model (Gregg & Sing, 1982) was used to calculate the specific surface area (SSA-N_2) and considered a limited maximum number of layers that can be formed in a pore (N):

$$V = V_m \frac{C(p/p^0)}{1-(p/p^0)} * \frac{1-(N+1)(p/p^0)^N + N(p/p^0)^{N+1}}{1+(C-1)(p/p^0)-C(p/p^0)^{N+1}} \quad (1)$$

where V is the amount of adsorbed gas at every relative pressure value (p/p^0), V_m is the monolayer capacity and C, according to the BET theory, gives an indication of the enthalpy of adsorption of the first adsorbed layer, that is the magnitude of the adsorbent-adsorbate interaction. The application of the BET equation was limited to the relative pressure range where the term $V_m(1-p/p^0)$ continuously increases with p/p^0 (ISO 9277, 2010). The parameters C and V_m were obtained using the Sorptomatic Software ADP 5 (Thermo Electron) and the SSA-N_2 calculated by multiplying the number of molecules adsorbed in V_m by the molecular surface area of N_2 (A_m= 0.162 nm^2). A wide pore diameter range can be detected with the BET method, from meso-pore (2–50 nm) to micro-pore (<2 nm) sizes, according to the IUPAC recommendations (Kaneko, 1994).

The same experimental equipment was used for the measurement of carbon dioxide adsorption isotherms at 273 K. The absence of chemisorption phenomena was verified by measuring both adsorption and desorption. The lack of a pronounced hysteresis indicated the absence of irreversible specific chemical bonds (de Jonge & Mittelmeijer-Hazeleger, 1996).

Micro-porosity was assessed for both CO_2 and N_2 using the Dubinin and Radushkevich (DR) equation (Gregg & Sing, 1982):

$$\log(V) = \log(V_0) - D\log^2(p^0/p) \quad (2)$$

where V is the volume of gas adsorbed per mass of soil, calculated as $V= n/\rho$, in which n is the mass of gas adsorbed and ρ is the liquid density of the gas used; V_0 is the total micro-pore volume and D is a parameter related to the structure of adsorbent and adsorbent-adsorbate affinity. The V_0 value was obtained as the intercept in a plot of $log(V)$ versus $log^2(p^0/p)$. The CO_2

monolayer equivalent surface area (SSA-CO_2) was obtained by multiplying the number of CO_2 molecules in V_0 by the CO_2 molecular surface area value (A_m), equal to 0.210 nm^2 as suggested by the standard ISO 9277 (2010). Because of the small interval of p/p^0 (<0.03) used, adsorption of CO_2 took place in the narrow micropores down to molecular dimensions and on the walls of super micropores (0.7–2 nm; Kaneko, 1994). The N_2 molecule diffusion at operative conditions is instead limited to pores having critical diameter of approximately 0.5 nm (de Jonge & Mittelmeijer-Hazeleger, 2000).

All surface area measurements were duplicated and all data obtained from the samples after NaClO oxidation were corrected by the mass loss during treatment.

Results

Soil properties and oxidation treatment

In the UT samples, the OC contents in the spodic N-CM horizons ranged from 25 to 37 g kg^{-1}, while all CM horizons had smaller amounts (on average 7.1±4.4 g kg^{-1}), with a maximum value of 14 g kg^{-1} in the P3-Bsm1 (Table 2). The NH_4-oxalate extractable metal concentrations were more variable; Fe_O values had a wider range (mean of 8.6 ±5.8 g kg^{-1}) than Al_O (mean of 4.2±2.1 g kg^{-1}) and no trend was found in relation to the horizon type. Large amounts of Mn_O occurred only in P2, with a concentration that reached 12.6 g kg^{-1} in the Bsm horizon, and Si_O had values greater than 1 g kg^{-1} in CM P3 horizons (Table 2). The chemical oxidation with 6% NaClO left a variable amount of resistant OC in the T samples (OC_{res}; from 0.8 to 8.9 g kg^{-1}, Table 2) thus removing up to 86% of the initial OC content. The amounts of OC_{res} showed a linear relationship with the OC in UT soil (r = 0.990; P <0.01) and, consequently the C losses were greater in the OM-richest N-CM horizons, as also confirmed by the mass loss data (4.6% and 1.3% of the initial mass in N-CM and CM on average, respectively). The oxidation of the most labile OM always resulted in an increase in, with ρ_s that changed from 2.57 to 2.64 g cm^3 on average, in UT and T samples, respectively (Table 2). The removal of the most labile OM explained almost totally the difference in density induced by treatment (R^2=0.891, P <0.001).

The molar concentration of OC_{res} was related to the moles of Fe_O and Al_O of the UT samples, but the relationship showed different trends whether the horizon was cemented or not (Figure 1). In the CM horizons there was always a larger metal to OC_{res} molar ratio (1.8 ± 0.5) than in the N-CM horizons (0.4 ± 0.6). The NaClO treatment typically caused the loss of more than half of the initial Fe_O and Al_O, although with some exceptions, with mean decreases of 77 and 69%, respectively (Table 2).

Pore characterization by N_2 and CO_2 adsorption

The samples differed in the amount of N_2 adsorbed at 77K, but all isotherms lacked a perfect correspondence to any IUPAC classification type (Gregg & Sing, 1982). Although they could not be strictly classified as type IV, because adsorption quantities at p/p^0 close to unit were unlimited (Kaneko, 1994), they generally showed a restricted hysteresis loop (Figure 2A). The P2-Bsm soil was an exception as the amounts of gas desorbed in both T and UT samples were much higher than in all other cases (Figure 2B). In all samples the loop shape was always recognized as being intermediary between a H3 and H4 type and the desorption branch showed the forced closure at similar pressure (p/p^0= about 0.42), which is characteristic of a random distribution of pores and an interconnected pore system (Echeverría *et al.*, 1999). The initial portion of the isotherms was an intermediate form between type II (indicative of the multilayer adsorption process in a non-porous or macro-porous system) and type I (typical of micro-porous solids).

When the specific surface area was calculated with Equation (1) and using the data obtained by N_2 adsorption (SSA-N_2), UT samples had varying surface areas (Table 3); the largest value was obtained in P2-Bsm (36.4 $m^2\ g^{-1}$), while the other samples had smaller values, from 1.9 to 14.5 $m^2\ g^{-1}$. After oxidation, the relative differences in SSA-N_2 between UT and T samples discriminated between N-CM and CM horizons, as seen in Figure 3. Only Bs/Bhs type horizons had an increase in SSA-N_2 (18% on the average) after the removal of labile OM, while in CM horizons the specific surface area always decreased. In all samples the micro-pore surface area calculated by Equation (2) followed the same trend as SSA (Table 3). Both before and after oxidation the surfaces were mainly composed of micro-pores, and the removal of the most labile OC always caused an increase in their relative proportion.

As shown by the two extreme examples reported in Figure 4, the CO_2 adsorption isotherms (Figure 4A) and derived DR plots (Figure 4B) differed in shape and volumes of adsorbed gas at every step of p/p^0, indicating that the abundance and characteristics of the narrow micro-pores differ between samples The linearity of the DR function obtained for sample P1-Bhs+Bs indicated a narrower size and a more homogeneous pore size distribution than the P2-Bsm sample (Figure 4B). For all samples, a limited branch of desorption was measured (data not shown), and the isotherms always showed a restricted or absent hysteresis. Although the detectable surface was limited to pores with diameter from molecular dimensions (0.3 nm) up to 0.7 nm, when the surface area was calculated with Equation (2) and the data obtained from CO_2 adsorption (SSA-CO_2), both UT and T had larger micro-porosity and total SSA than those

measured with N_2 (Table 3). The only exception was P2-Bsm, in which a larger surface area was measured by N_2 than by CO_2. The calculated SSA-CO_2 in N-CM horizons was always larger than in CM ones, with mean values of 39 ±4 and 11 ±5 m^2 g^{-1}, respectively. After oxidation the SSA-CO_2 always diminished (Table 3) and, although the relative decrease varied among samples (from 3 to 54 %), the difference in m^2 g^{-1} between UT and T was linked to the amount of oxidized OC (r = 0.915, P <0.01; Figure 5A). Moreover, the SSA obtained by CO_2 was strongly related to the OC in both UT and T samples (Figure 5B, r =0.981 and 0.958, respectively, P <0.05). The two functions in Figure 5B had equivalent intercept values (4.35 and 4.36 m^2g^{-1}, respectively), and the slope of the oxidized samples was more than twice that of the UT samples.

Discussion

In this work we compared the porosity characteristics of NaClO-resistant and labile OM, taking into account CM and N-CM podzolic horizons in order to have a gradient in development of metal-organic interactions. Thus we compared the chemical and physical characteristics of the soils and the variations in gas accessibility before and after oxidation treatment.

Effect of oxidation treatment on soil properties

Cementation was always well expressed and enhanced by the large volume of coarse fragments (Lapen & Wang, 1999). However, in the case of P2 and P3 the Bsm samples fulfil all WRB diagnostic criteria for ortstein, while in P1 the spodic index was too small, both with Bsm and CBm. Even if induration in acidic deep horizons may develop independently from the podzolization process, as in the case of glacial compaction, clay bridging or Si cementation, both field properties and the analogous behaviour of the cemented horizons of P1 with respect to the other CM horizons (Figure 1) indicate that podzolization is the main pedogenic process. The colour of the cemented horizons is related to the amounts of specific metal and to OM (Wilson & Righi, 2010). The strong presence of Mn_O in P2, whose parent material included Mn-rich calcschists, resulted in the very dark brown colour of the P2 Bsm horizon. In P3, although the amount of Si_O was relatively large, the quantity of iron in CM samples was sufficient to dominate the hue (Table 1). In P1, the CM horizons had a hue comparable to that found in cemented horizons of North America Spodosols (Freeland & Evans, 1993).

The OC concentrations in N-CM spodic horizons were comparable to those normally found in non-cemented deep layers of NW Italian forest soils (Bonifacio *et al.*, 2011), and the smaller concentrations in CM horizons were in agreement with those of other Podzols with ortstein

(Bockheim, 2011). The proportions of NaClO-labile OC were always more than 50% and similar to those of acidic forest soils (Kaiser *et al*., 2002; Mikutta *et al*., 2006). No specific trend in the proportion of the most labile C down the profile was observed, because of the strong dependence of C losses on the sample OC contents.

The OM content affects soil ρ_s substantially because of the density of organic materials which is reported to range from about 1 to 1.9 g cm^{-3} (Mayer *et al*., 2004) depending mainly on the elemental composition of organic compounds. The very good relationship between the variation in density and the amounts of NaClO-labile OC indicated a remarkable homogeneity of this OM pool.

Figure 1 shows that the amount of OC_{res}, is correlated with the occurrence of Al_O and Fe_O in the samples, thus confirming the importance of Al and Fe interactions in podzolic illuvial layers and suggesting a relationship between illuviated OM and NaClO-resistant OC. The importance of metal-organic interaction in affecting the amount of resistant OM toward oxidation was noted by Mikutta & Kaiser (2011), whose results suggested that although the NaClO-removable fraction was not directly linked to the biodegradable fraction, the treatment caused an enrichment of the OM preferentially bound to oxides. However, the oxalate extractable metals to OC_{res} molar ratio differed markedly depending on whether the horizon was cemented or not, with larger values in CM horizons than in N-CM samples. This difference between horizon types may be related to the modification of OM forms occurring with podzolization. Buurman & Jongmans (2005), with thin section observations, pointed out that strongly cemented ortstein is made up by welded and illuvial organic coatings, which are composed of uniform and continuous colloidal-sized materials. Instead, the B horizons of N-CM well drained horizons yielded OM resulting also from the transformations of non-illuvial materials (Wilson & Righi, 2010). This indicates that OM changes toward a more homogeneous distribution of stabilized organic forms on mineral surfaces in the ortstein horizons.

Kaiser & Guggenberger (2003) suggested that OM may be stabilized by the formation of multiple bonds per molecule at the micropore mouths. Consequently, the illuvial organic coatings, having a more intimate association with mineral surfaces, should be characterized by a larger metal to OC molar ratio. As the interactions between OM and mineral surfaces differ in cemented and non-cemented horizons, surface properties should also vary accordingly.

Effect of OM removal on soil surface features

Nitrogen adsorption gave small SSA values, with much variability among samples (Table 3). Podzol B horizons are typically characterized by coarse texture and a relatively large presence of

OM, which generally translate into small surface areas. On the other hand, even small amounts of Al and Fe (hydr)oxides strongly influences surface properties because of the large SSA-N_2 of their poorly crystalline forms (Cornell & Schwertmann, 1996). We observed a synergic effect of several soil features on the final SSA-N_2 values, that did not show any direct relationship with the amount of OC_{res} or with the oxalate-extractable metals (P >0.05 in both cases). This is in contrast with the results of previous studies on soils (Kaiser & Guggenberger, 2003) and marine sediments (Mayer, 1999), in which direct inverse relationships between the SSA properties and the contents of mineral associated OM were reported. The variation of SSA-N_2 values upon oxidation was instead linked to the horizon type, with a clear discrimination between N-CM and CM horizons (Figure 3). In contrast to previous findings (Bonifacio *et al*., 2013), the expected increase in SSA was present in all N-CM horizons, and in CM horizons a decrease in SSA was always observed. This occurred independently of the degree of horizon development, their initial OM content, OM decrease upon oxidation, and oxalate-extractable metal losses. These results confirm the greater effectiveness of 6% NaClO than the 2% solution used previously to remove the small SSA OM component, but also indicated that the weaker treatment better discriminated among different steps of spodic horizons development. The balance in surface area before and after oxidation gives indications of whether the newly exposed surfaces are mainly mineral or organic. Consequently, in N-CM horizons the increase in SSA-N_2 indicates the prevalence of mineral surfaces exposed after oxidation (Figure 6A). In the CM horizons the decrease of SSA-N_2 probably reflects the exposure of homogenously distributed stabilized OM, characterized by a surface with more N_2-inaccessible pores (<0.5 nm), further indicating the occurrence of illuvial organic coverings in CM podzolic horizons (Wilson & Righi, 2010).

When estimated by N_2 adsorption, micro-porosity (<2 nm) always dominated total SSA-N_2 indicating the importance of the smallest sized fraction in all analysed samples independently of the absolute meso-porosity, and the relative proportion of the <2 nm surface always increased after oxidation. This indicated that the newly exposed surfaces in both N-CM and CM samples, either organic or mineral, were rich in micro-porosity. As a consequence, no relationship was found between micro-pores and OC, as the <2 nm pores are also typical of the mineral phase (Aringhieri, 2004).

The micro-pore surface obtained with CO_2 was generally much larger than with N_2 (Table 3). Because of greater diffusivity, only the smallest sized micro-pores are measured with CO_2 (de Jonge & Mittelmeijer-Hazeleger, 1996). Our results thus confirm the importance of molecular-dimensioned pores (< 0.5 nm) in all podzolic soil samples but P2-Bsm. The smaller SSA-CO_2 values in comparison to the measured SSA-N_2 found in this sample indicated that a

micro-pore class of at least three molecules wide (about 1.5 nm) dominated both before and after oxidation. Using the standard operative conditions, in fact, the amount of adsorbed N_2 is larger in the presence of super micropores (1.5-2 nm), because CO_2 molecules can only adsorb on the pore walls, while N_2 completely fill their volume (Mittelmeijer-Hazeleger, 2006).

The good linear relationships reported in Figure 5B suggest that the SSA-CO_2 was strongly affected by the presence of OC in both UT and T samples, regardless of the specific micro-pore main class. The similarity of the intercepts of two relations confirmed the selectivity of the oxidation treatment that did not have any effect on the mineral phases (Zimmermann *et al.*, 2007), at least when small micro-porosity is concerned, and indicated a mineral specific surface area of around 4.4 m^2 g in these samples. The variations in SSA-CO_2 between UT and T samples were caused by the release of OC upon oxidation (91% of explained variance), while the clear relationship between SSA-CO_2 and C contents in both UT and T samples (Figure 5B) suggested that both labile and stabilized OM affect the SSA of small-sized pores. The relationships between SSA-CO_2 and OC in UT and T samples, however, differed markedly in slope, thus clearly pointing to important structural differences in oxidized and stabilized OM pools. In fact OC had a more pronounced effect (twice as much) on the SSA-CO_2 in the T samples than in the UT samples (Figure 5B), indicating a larger presence of small micro-pores in the stabilized OM than in the labile pool. However, the occurrence of a good relationship for both UT and T samples indicated that each OM pool was homogeneous when the micro-porosity was measured with CO_2, independently of the morphological characteristic of horizons.

Assuming therefore that both labile and stabilized OM pools had homogeneous elemental composition, we transformed the OC to OM contents by multiplying by either 2 or 1.5 (Table 4), thus taking into account the widest reported C composition of soil OM (Kasozi *et al.*, 2009; Bhatti & Bauer, 2002). We were therefore able to calculate the SSA of small micropores (*SSA–CO_2*) of both OM pools with an additive model as follows:

$$SSA-CO_2\ UT = SSA-CO_2\ OM_{ox} \cdot x_{ox} + SSA-CO_2\ OM_{res} \cdot x_{res} + 4.4 \cdot x_{\min} \quad (3)$$

where x_{ox} and x_{res} were the weight fractions of oxidized and NaClO-resistant OM pools, while x_{min} was the weight fraction of mineral material in the sample, which had a SSA-CO_2 of 4.4 m^2 g^{-1} as found previously. The $SSA - CO_2\ OM_{ox}$ and $SSA - CO_2\ OM_{res}$ values were the micro-pore surface areas of NaClO-labile and resistant OM, respectively. The $SSA - CO_2\ OM_{ox}$ was obtained with a similar additive model considering the mineral and resistant OM fractions together ($x_{min+res}$) and the measured SSA-CO_2 of the T samples ($SSA - CO_2\ T$):

$$SSA-CO_2\ UT = SSA-CO_2\ OM_{ox} \cdot x_{ox} + SSA-CO_2\ T \cdot x_{\min+res} \quad (4)$$

The $SSA - CO_2\ OM_{res}$ values were determined with Equation (3) and using the calculated $SSA - CO_2\ OM_{ox}$ by applying Equation (4). Using this method we could therefore confirm that in our samples the two OM pools showed marked differences in the micro-pore surface measured by CO_2 adsorption, as on the average the SSA-CO_2 varied from 287 to 379 $m^2\ g^{-1}$ as a function of C percentage in labile OM, while in the stabilized OM it was 1383-1856 $m^2\ g^{-1}$ (Table 4, Figure 6B). Organic matter in Podzols is reported to be composed of up to 62–67% C (Kasozi *et al*., 2009), thus the largest calculated values are the most plausible. The calculated SSA-CO_2 of labile OM was more variable than that of the stabilized pool (Table 4), but in both cases it was much greater than previously measured data (80-150 $m^2\ g^{-1}$, de Jonge & Mittelmejier-Hazeleger, 2000). It is worth noting, however, that the materials used in the latter experiment were peat, organic layers and a synthetic humic acid, thus not representative of OM in Podzol B horizons, for either labile or stabilized forms. OM in podzolic B horizons accumulates due to a chemical selection process thus the large SSA data obtained are in agreement with an expected much greater reactivity than that of poorly sorted and less transformed materials of organic layers.

Conclusions

In podzolic B horizons, the morphological characteristics and the process of metal-organic translocation and immobilization sharply affect the OM surface properties and structural organization. Organic matter is characterized by a large degree of small-porosity, but the stabilization through association with mineral surfaces induces a considerable increase of <0.5 nm pores in comparison to the NaClO-labile forms.

The non-cemented and cemented illuvial horizons do not differ in the strength of association between organics and minerals, but in the relative amount and arrangement of organic matter pools. In non-cemented horizons, the NaClO-resistant OM is present as patches on mineral surfaces, while NaClO-labile OM occurs in a bulky open configuration, covering both mineral phases and some patches of the stabilized OM surfaces. In cemented horizons, illuvial OM coatings are homogeneously spread over mineral surfaces. As illuvial OM is are not removed by oxidation, organic surfaces prevail on inorganic ones when the labile OM is removed. As a consequence, the SSA measured by CO_2 adsorption is large in both cemented and non-cemented B horizons and directly dependent on the relative amount of NaClO-stabilized OM. Because of the limited diffusion of N_2 into the small micro-pores, instead, the prevalence of mineral or stabilized organic phases determines the increase or decrease in SSA-N_2 after oxidation.

These results indicate that, in illuvial podzolic B horizons, the intimate association with mineral surfaces causes a remarkable variation of the OM micro-pore structure which potentially

affects C cycling. They also show the need for further investigations to verify if this is a typical feature of illuvial OM or if other less specific pedogenic processes may induce similar characteristics.

Acknowledgements

M. Catoni thanks the Società Italiana di Scienza del Suolo for a mobility grant that allowed her to stay at the Van 't Hoff Institute of Molecular Sciences, University of Amsterdam.

References

Aringhieri, R. 2004. Nanoporosity characteristics of some natural clay minerals and soils. *Clays & Clay Minerals*, **52,** 700-704.

Bhatti, J.S. & Bauer, I.E. 2002. Comparing loss-on-ignition with dry combustion as a method for determining carbon content in upland and lowland forest ecosystems. *Communications in Soil Science & Plant Analysis*, **33,** 3419-3430.

Bockheim, J. 2011. Distribution and genesis of ortstein and placic horizons in soils of the USA: a review. *Soil Science Society of America Journal*, **75,** 994-1005.

Bonifacio, E., Falsone, G. & Petrillo, M. 2011. Humus forms, organic matter stocks and carbon fractions in forest soils of North-western Italy. *Biology & Fertility of Soils*, **47,** 555-566.

Bonifacio, E., Catoni, M., Falsone, G., Said-Pullicino, D. & Celi L. 2013. Evolution of surface properties and organic matter stabilization in podzolic B horizons as assessed by nitrogen and phosphate sorption. *Biology & Fertility of Soils*, **49,** 505-516.

Buurman, P. & Jongmans, A.G. 2005. Podzolization and soil organic matter dynamics. *Geoderma*, **125,** 71-83.

Chiou, T.C., Lee, J.F. & Boyd, S.A. 1990. The surface area of soil organic matter. *Environmental Science & Technology*, **24,** 1164–1166.

Cornell, R.M. & Schwertmann, U. 1996. *The Iron Oxides*. WILEY-VCH, Weinheim, Germany.

de Jonge, H. & Mittelmeijer-Hazeleger, M.C. 1996. Adsorption of CO_2 and N_2 on soil organic matter: nature of porosity, surface area, and diffusion mechanisms. *Environmental Science &Technology*, **30,** 408-441.

de Jonge, H., de Jonge, L.W. & Mittelmeijer-Hazeleger, M.C. 2000. The microporous structure of organic and mineral soil materials. *Soil Science*, **165,** 99-108.

Echeverría, J.C., Morera, M.T., Mazkiarán, C. & Garrido, J.J. 1999. Characterization of the porous structure of soils: Adsorption of nitrogen (77 K) and carbon dioxide (273 K), and mercury porosimetry. *European Journal of Soil Science*, **50,** 497-500.

Freeland, J.A. & Evans, C.V. 1993. Genesis and profile development of Success soil, Northern New Hampshire. *Soil Science Society of America Journal*, **57,** 183-191.

Ghosh, K. & Schnitzer, M. 1980. Macromolecular structure of humic substances. *Soil Science*, **129**, 266-276.

Gregg, S.J. & Sing, K.S.W. 1982. *Adsorption, Surface Area and Porosity*, Academic Press, London, UK.

ISO 9277. 2010. *Determination Of The Specific Surface Area Of Solids By Gas Adsorption - BET Method*. ISO, Geneva, Switzerland.

IUSS Working Group WRB. 2006. *Food and Agriculture Organization: World Reference Base for Soil Resources. A Framework For International Classification, Correlation And Communication. World Soil Resources Report No.103*, FAO, Rome, Italy.

Jastrow, J.D., Amonette, J.E. & Bailey, V.L. 2007. Mechanisms controlling soil carbon turnover and their potential application for enhancing carbon sequestration. *Climatic Change*, **80,** 5-23.

Kaiser, K. & Guggenberger, G. 2003. Mineral surfaces and soil organic matter. *European Journal of Soil Science*, **54,** 219–236.

Kaiser, K. & Guggenberger, G. 2007. Sorptive stabilization of organic matter by microporous goethite: sorption into small pores vs. surface complexation. *European Journal of Soil Science*, **58**, 45–59.

Kaiser, K., Eusterhues, K., Rumpel, C., Guggenberger, G. & Kögel-Knabner, I. 2002. Stabilization of organic matter by soil minerals – investigations of density and particle-size fractions from two acid forest soils. *Journal of Plant Nutrition & Soil Science*, **165,** 451–459.

Kaneko, K. 1994. Review: determination of pore size and pore size distribution. 1. Adsorbents and catalysts. *Journal of Membrane Science*, **96,** 59-89.

Kasozi, G.N., Nkedi-Kizza, P. & Harris, W.G. 2009. Varied carbon content of organic matter in Histosols, Spodosols and carbonatic soils. *Soil Science Society of America Journal*, **73,** 1313-1318.

Kleber, M., Mikutta, R., Torn, M.S. & Jahn, R. 2005. Poorly crystalline mineral phases protect organic matter in acid subsoil horizons. *European Journal of Soil Science*, **56,** 717-725.

Kleber, M., Sollins, P. & Sutton, R. 2007. A conceptual model of organo-mineral interactions in soils: self-assembly of organic molecular fragments into zonal structures on mineral surfaces. *Biogeochemistry* , **85**, 9-24.

Lal, R. 2008. Sequestration of atmospheric CO_2 in global carbon pools. *Energy & Environmental Science*, **1,** 86-100.

Lapen, D.R. & Wang, C. 1999. Placic and ortstein horizon genesis and peatland development, south-eastern Newfoundland. *Soil Science Society of America Journal*, **63,** 1472-1482.

Lehmann, J., Solomon, D., Kinyangi, J., Dathe, L., Wirick, S. & Jacobsen, C. 2008. Spatial complexity of soil organic matter forms at nanometre scales. *Nature Geoscience*, **1**, 238-242.

Mayer, L.M. 1999. Extent and coverage of mineral surfaces by organic matter in marine sediments. *Geochimica et Cosmochimica Acta*, **63,** 207-215.

Mayer, L.M., Schick, L.L., Hardy, K.R., Wagai, R. & McCarthy, J. 2004. Organic matter in small mesopores in sediments and soils. *Geochimica et Cosmochimica Acta*, **68,** 3863-3872.

Mikutta, R., & Kaiser, K. 2011. Organic matter bound to mineral surfaces: resistance to chemical and biological oxidation. *Soil Biology & Biochemistry*, **43,** 1738-1741.

Mikutta, R., Kleber, M., Torn, M.S. & Jahn, R. 2006. Stabilization of soil organic matter: association with minerals or chemical recalcitrance? *Biogeochemistry*, **77,** 25-56.

Mittelmeijer-Hazeleger, M.C. 2006. *Understanding adsorption in micropores. A study of carbons, soils and zeolites*. PhD dissertation, Universiteit van Amsterdam, Amsterdam.

Sasaki, O., Kanai, I., Yazawa, Y. & Yamaguchi, T. 2007. Relationship between the chemical structure of humic substances and their hygroscopic properties. *Annals of Environmental Science*, **1,** 17-22.

Schmidt, M.W.I., Torn, M.S., Abiven, S., Dittmar, T., Guggenberger, G., Janssens, I.A. *et al*. 2011. Persistence of soil organic matter as an ecosystem property. *Nature,* **478**, 49-56.

Schwertmann, U. 1964. Differenzierung der Eisenoxide des Bodens durch Extraktion mit Ammoniumoxalat-lösung. *Zeitschrift für Pflanzenernährung Düngung und Bodenkunde*, **105,** 194-201.

von Lützow, M., Kögel-Knabner, I., Ludwig, B., Matzner, E., Flessa, H., Ekschmitt, K., *et al*. 2008. Stabilization mechanisms of organic matter in four temperate soils: Development and application of a conceptual model. *Journal of Plant Nutrition & Soil Science,* **171,** 111–124.

Wang, K. & Xing, B. 2005. Structural and sorption characteristics of adsorbed humic acid on clay minerals. *Journal of Environmental Quality,* **34**, 342-349.

Wilson, M.A. & Righi, D. 2010. Spodic materials. In: *Interpretation of Micromorphological Features of Soils and Regoliths* (eds G. Stoops, V. Marcelino and F. Mees), pp. 251-273. Elsevier, Amsterdam, the Netherlands.

Zimmermann, M., Leifeld, J., Abiven, S., Schmidt, M.W.I. & Fuhrer, J. 2007. Sodium hypochlorite separates an older soil organic matter fraction than acid hydrolysis. *Geoderma*, 139, 171–179 .

Table 1 Site characteristics and morphological properties of the studied horizons.

Profile	Location	Coordinates (32T)	Altitude	Classification	Horizon sequence[a]	Sample	Depth	Munsell Colour	Skeleton[c]	Structure[d]
		UTM WGS84	/m a.s.l.	WRB			/cm	crushed and moist	/%	
P1	Chiusa Pesio	03942330E, 4895146 N	1400	Albic Podzol	O-A-E-*Bhs*-*Bs*-*Bsm*-*CBm*	Bhs+Bs[b]	25-30	7.5YR 3/3	85	w, m, sbk
						Bsm	30-45	10YR 5/4	90	Cemented
						CBm	45-65	2.5Y 5/4	90	Cemented
P2	Gran San Bernardo	0356811E, 5081660N	2280	Ortsteinic Albic Podzol	A-E-*Bs*-*Bsm*-Cm	Bs	10-20	10YR 4/3	75	vw, m, sbk
						Bsm	20-30	7.5YR 2.5/2	80	Cemented
P3	Staffal	0407445E, 5074613N	1995	Ortsteinic Albic Podzol	O-AE-E-EBh-*Bs*-*Bsm1*-*Bsm2*-Cm	Bhs	50-70	7.5YR 3/3	90	w, f, sbk
						Bsm1	70-110	7.5YR 4/8	95	Cemented
						Bsm2	110-150	10YR 5/6	95	Cemented

[a] Italics indicate the horizons analysed in this study.
[b] Sampled and analysed together.
[c] field estimate.
[d] Structure: vw= very weak, w=weak, m=medium; f=fine, m=medium; sbk=subangular blocky.

Table 2 Characteristics of untreated (UT) and NaClO-treated (T) of non-cemented (N-CM) and cemented (CM) B horizons. In parentheses, the standard deviation is given.

Profile	Cementation	Sample		OC	ρ_s[a]	AlO	FeO	MnO	SiO	Mass loss[b]	SI
				/g kg^{-1}	/g cm^{-3}	/g kg^{-1}	/g kg^{-1}	/g kg^{-1}	/g kg^{-1}	/%	/%
P1	N-CM	Bhs+Bs	UT	37.3 (4.8)	2.40	4.57 (0.08)	12.75 (0.09)	0.01 (0.00)	0.15 (0.03)	4.46 (0.44)	1.09
			T	8.9 (1.3)	2.51	2.27 (0.04)	7.78 (0.05)	0.01 (0.00)	0.12 (0.04)		
	CM	Bsm	UT	6.6 (0.0)	2.57	2.01 (0.02)	2.22 (0.01)	0.03 (0.00)	0.30 (0.04)	1.25 (0.50)	0.31
			T	0.9 (0.2)	2.60	1.06 (0.02)	1.13 (0.02)	0.02 (0.00)	0.12 (0.03)		
	CM	CBm	UT	4.0 (0.2)	2.58	1.75 (0.03)	0.66 (0.00)	0.09 (0.01)	0.40 (0.02)	0.62 (0.48)	0.21
			T	0.8 (0.1)	2.64	1.35 (0.02)	0.57 (0.01)	0.05 (0.00)	0.66 (0.02)		
P2	N-CM	Bs	UT	24.9 (3.1)	2.48	2.43 (0.02)	13.45 (0.10)	0.34 (0.02)	0.04 (0.01)	3.95 (0.43)	0.92
			T	6.0 (0.3)	2.58	1.91 (0.03)	11.84 (0.08)	0.27 (0.02)	0.12 (0.01)		
	CM	Bsm	UT	8.7 (0.4)	2.68	5.69 (0.06)	14.08 (0.09)	12.59 (0.02)	0.17 (0.01)	1.98 (0.90)	1.27
			T	2.4 (0.1)	2.74	6.13 (0.06)	16.36 (0.05)	15.48 (0.01)	0.30 (0.02)		
P3	N-CM	Bhs	UT	36.9 (0.3)	2.56	4.43 (0.04)	13.17 (0.04)	<0.01 (0.00)	0.13 (0.03)	5.42 (0.33)	1.10
			T	7.8 (0.6)	2.68	3.16 (0.03)	17.11 (0.05)	<0.01 (0.00)	0.21 (0.03)		
	CM	Bsm1	UT	13.7 (1.4)	2.64	8.08 (0.00)	10.07 (0.02)	0.01 (0.00)	1.79 (0.05)	1.85 (0.47)	1.31
			T	3.7 (0.4)	2.70	5.53 (0.03)	9.47 (0.01)	0.01 (0.00)	1.32 (0.04)		
	CM	Bsm2	UT	2.4 (0.1)	2.66	4.44 (0.02)	2.15 (0.02)	0.03 (0.00)	1.52 (0.04)	0.62 (0.63)	0.55
			T	1.1 (0.1)	2.70	3.82 (0.01)	1.82 (0.01)	0.03 (0.00)	1.41 (0.01)		

[a] Standard deviation <0.01 for all samples.

[b] recorded mass loss upon NaClO oxidation.

All T samples were corrected for the mass loss upon NaClO oxidation.

OC: organic carbon; ρ_s: soil particle density; Al_O, Fe_O, Mn_O, and Si_O: NH_4-oxalate extractable elements; SI: Spodic Index, $0.5Fe_O+Al_O$;

Table 3 Surface properties of untreated (UT) and NaClO-treated (T) B horizons, the T sample data are corrected for the weight loss upon NaClO treatment. The standard deviation is given in parentheses.

Profile	Cementation	Sample		SSA-N_2 /m^2 g^{-1}	N_2 – micro-pore surface /m^2 g^{-1}	SSA-CO_2 /m^2 g^{-1}
P1	N-CM	Bhs+Bs	UT	5.7 (0.1)	4.2 (0.0)	43.3 (0.8)
			T	7.2 (0.3)	5.6 (0.4)	22.5 (0.5)
	CM	Bsm	UT	3.0 (0.2)	2.2 (0.1)	8.6 (0.2)
			T	2.1 (0.0)	1.7 (0.0)	4.0 (0.1)
	CM	CBm	UT	1.9 (0.3)	1.4 (0.1)	6.3 (0.2)
			T	1.7 (0.3)	1.4 (0.1)	3.9 (0.0)
P2	N-CM	Bs	UT	6.9 (1.8)	5.1 (0.8)	35.2 (0.3)
			T	8.1 (2.5)	6.7 (1.1)	21.7 (0.1)
	CM	Bsm	UT	36.4 (3.3)	32.9 (2.4)	13.4 (0.2)
			T	28.8 (4.5)	28.6 (2.8)	11.6 (0.2)
P3	N-CM	Bhs	UT	14.5 (1.0)	11.6 (0.7)	38.4 (1.1)
			T	16.0 (0.3)	13.5 (0.1)	24.7 (0.6)
	CM	Bsm1	UT	9.7 (1.9)	8.1 (0.7)	19.2 (0.2)
			T	8.7 (2.1)	7.4 (0.6)	14.1 (0.0)
	CM	Bsm2	UT	2.5 (0.1)	2.0 (0.0)	8.7 (0.3)
			T	2.1 (0.0)	1.8 (0.0)	8.5 (0.1)

Table 4 Labile and resistant OM amounts calculated by multiplying 2.0 (Min) and 1.5 (Max) the OC values and SSA-CO2 calculated with Equations (3) and (4).

Profile	Cementation	Sample					Calculated SSA-CO_2					
			NaClO- labile OM		NaClO-resistant OM		NaClO- labile OM		NaClO- resistant OM		Total OM	
			Min	Max	Min	Max	Min	Max	Min	Max	Min	Max
			/%				/m^2 g^{-1}					
P1	N-CM	Bhs+Bs	5.7	4.3	1.8	1.3	389	512	959	1297	526	699
	CM	Bsm	1.1	0.8	0.2	0.1	408	543	nd	nd	nd	nd
	CM	CBm	0.7	0.5	0.2	0.1	375	498	nd	nd	nd	nd
P2	N-CM	Bs	3.8	2.8	1.2	0.9	378	497	1385	1863	622	827
	CM	Bsm	1.2	0.9	0.5	0.4	158	207	1448	1935	522	695
P3	N-CM	Bhs	5.8	4.4	1.6	1.2	260	338	1231	1666	465	618
	CM	Bsm1	2.0	1.5	0.7	0.5	267	352	1310	1754	544	725
	CM	Bsm2	0.3	0.2	0.2	0.2	63	82	1968	2624	902	1201
		Mean	/m^2 g^{-1}				287	379	1383	1856	597	794
		Standard deviation	/m^2 g^{-1}				125	166	333	437	158	210
		CV	/%				44	44	24	24	26	26

nd: not determined

Figure 1 Relationship between oxalate-extractable Fe and Al and resistant OC (OC_{res}) in non-cemented (N-CM) and cemented (CM) horizons. Lines are drawn only to show the two different trends. Vertical and horizontal bars represent standard deviations.

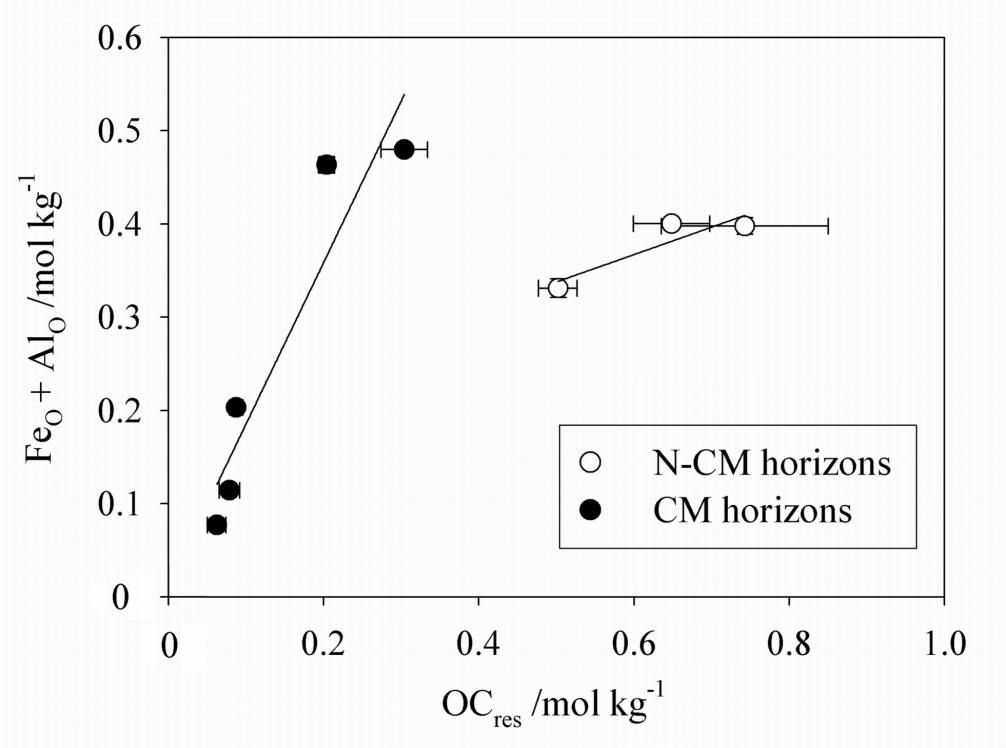

Figure 2 Representative N_2 adsorption and desorption isotherms of untreated B horizons from (a) profile 3 (non-cemented, UT-P3 Bhs), and (b) profile 2, (cemented, UT-P2 Bsm).

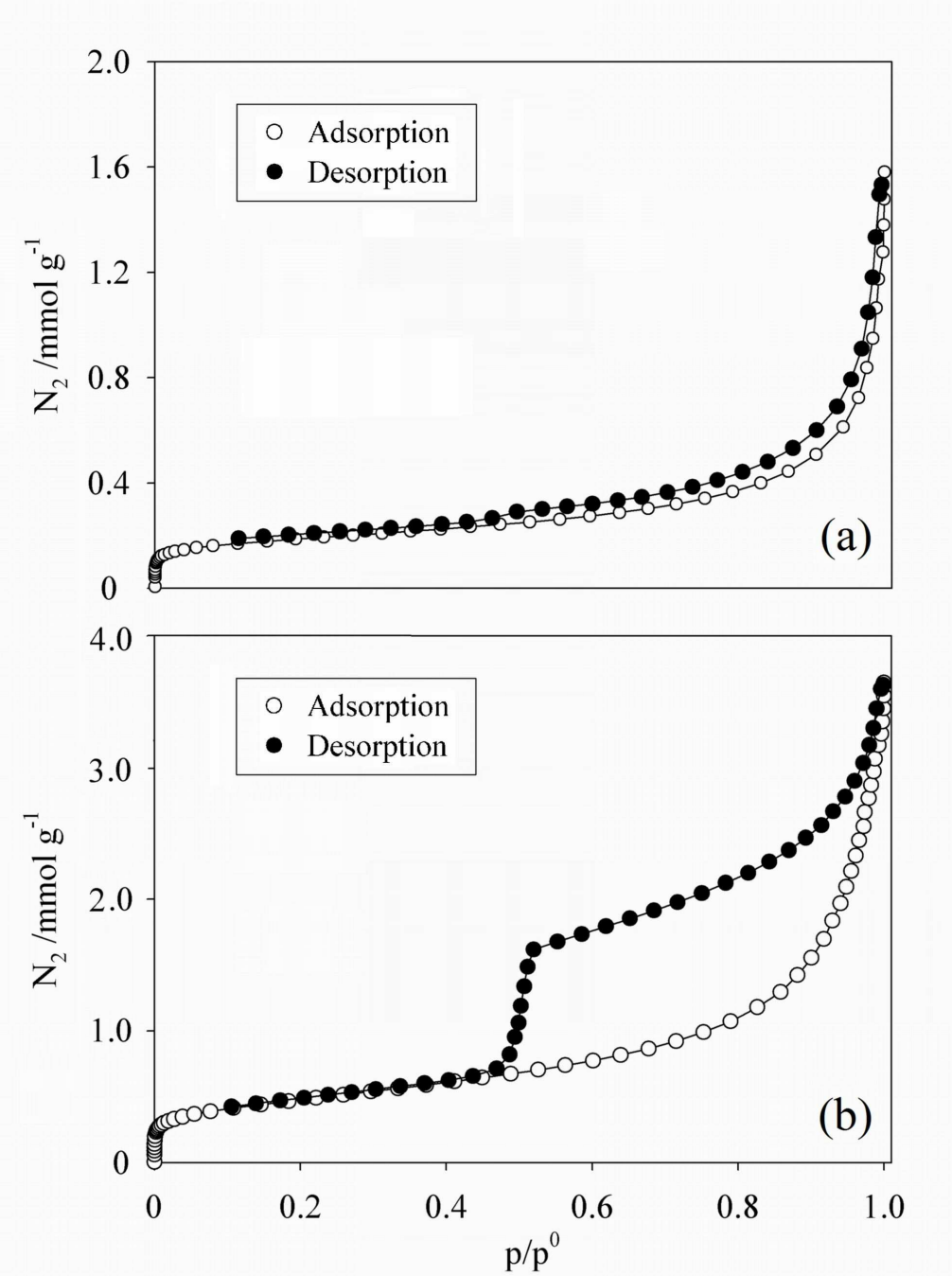

Figure 3 Relative variations in specific surface area by N_2 adsorption (SSA-N_2) upon oxidation with NaClO. Bars represent standard deviations of the difference in SSA before and after the NaClO treatment.

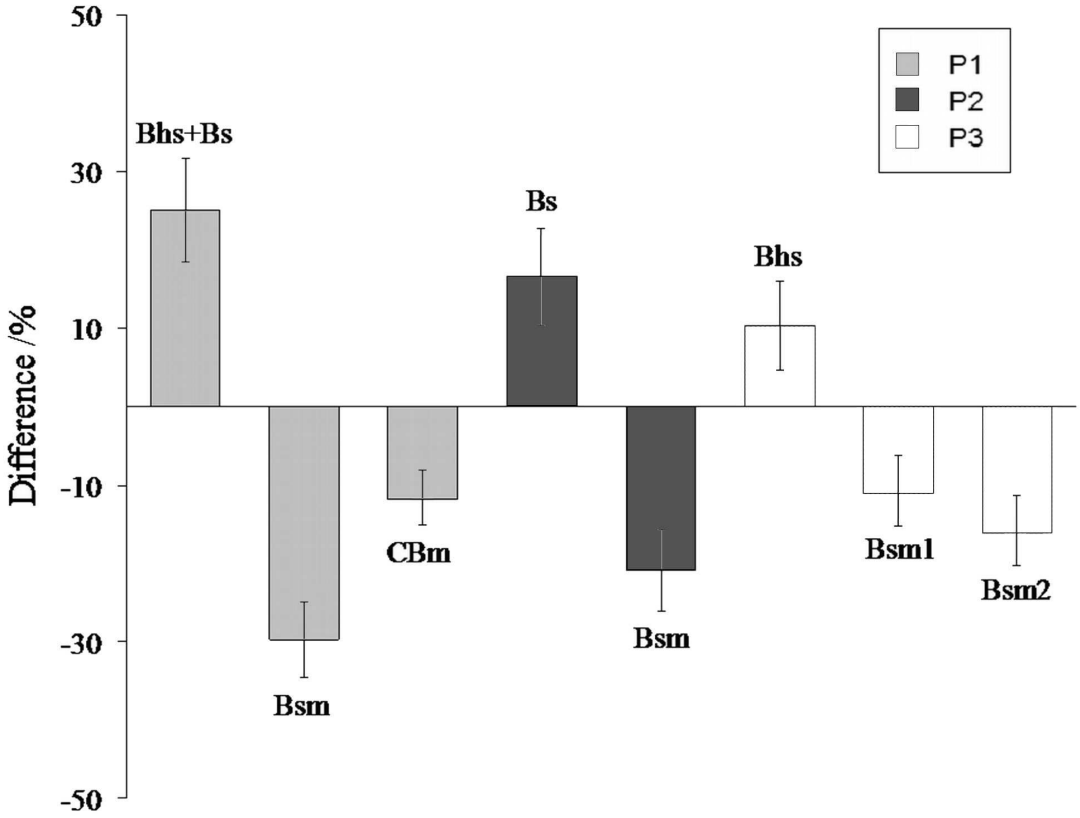

Figure 4 Representative (a) CO_2 adsorption isotherms of untreated B horizons from profile 1 (UT- P1 Bhs+Bs), and profile 2 (UT – P2 Bsm) and (b) their relative Dubinin-Radushkevich plots.

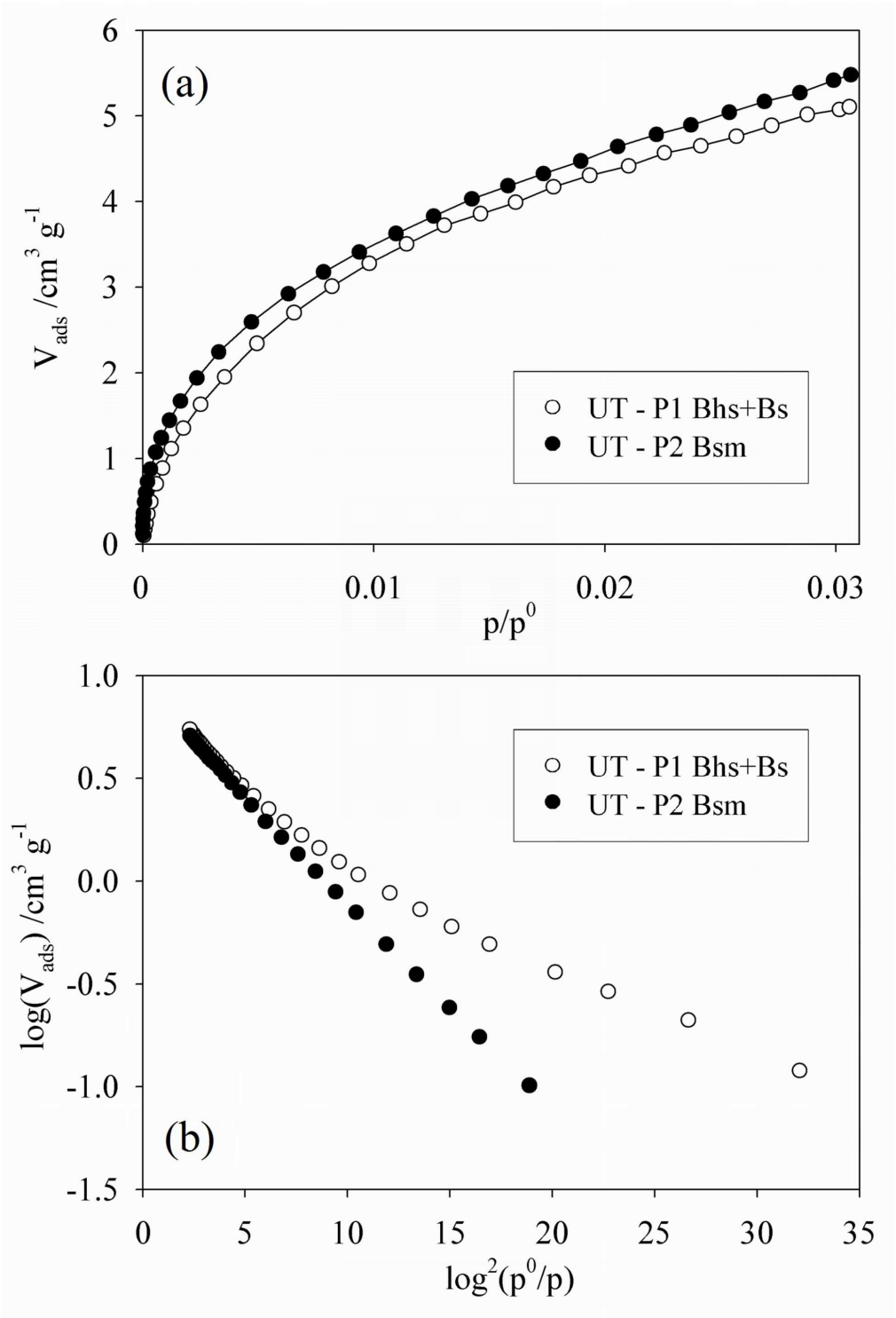

Figure 5 Relationships between organic carbon and specific surface area obtained by CO_2 adsorption (SSA-CO_2). (a) effect of OM removal (NaClO-labile OC) on SSA-CO_2 upon oxidation, (b) effect of organic carbon (OC) contents on SSA-CO_2 in untreated (UT, open symbols), and treated samples (T, closed symbols). Fitting lines represent linear correlation equations (r=0.981 and 0.958 for UT and T samples, respectively, OC_{res} is NaClO-resistant OC). Vertical and horizontal bars are standard deviations.

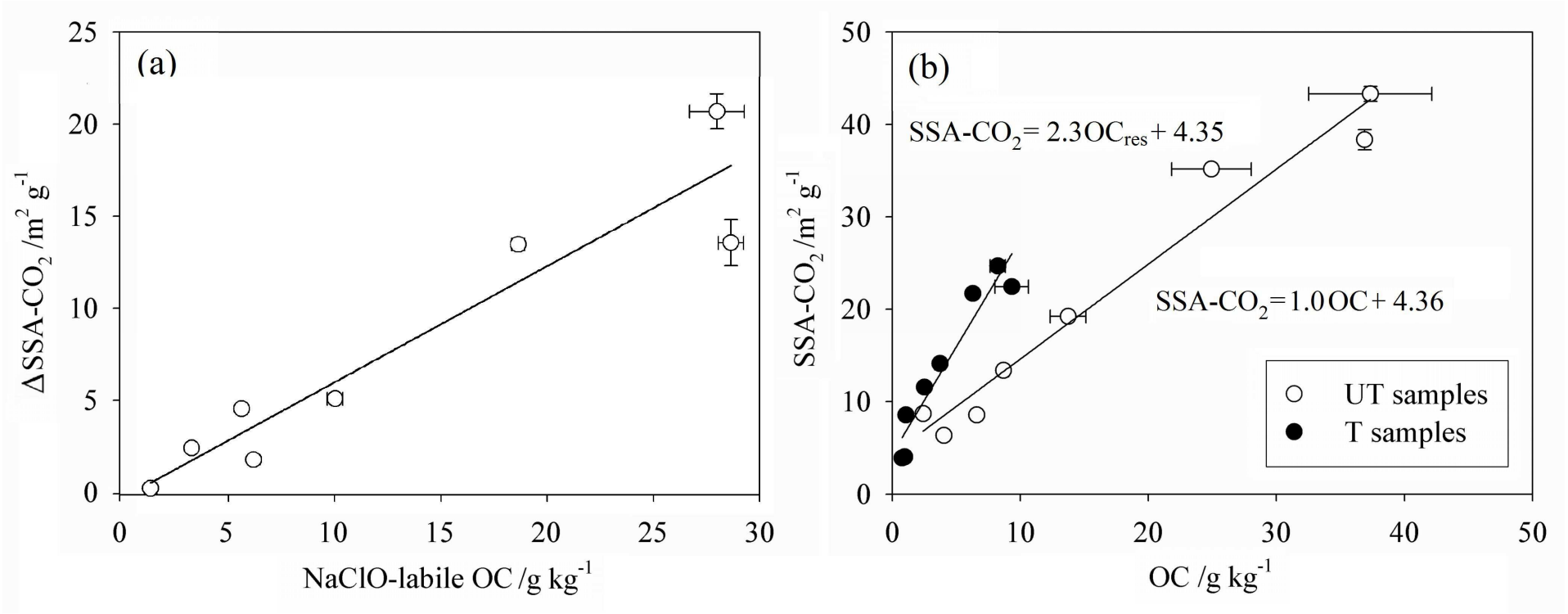

Figure 6 Schematic representation of spatial arrangement and surface properties of organic matter in non-cemented (N-CM) and cemented (CM) podzolic B horizons as deduced from the N_2 (a) and CO_2 (b) adsorption data.